Zachary Mazlan

University of Washington
School of Oceanography

An investigation into flow features at Cross Seamount, Hawaii

OC443 Senior Cruise Manuscript

Zachary Mazlan
Email: zmaz@uw.edu

Acknowledgements

The author would like to thank Charles Eriksen for his time, patience and tutelage during the preparation of this manuscript; without which this work would not have been possible. The author would also like to acknowledge the invaluable contributions of Rick Keil, Rika Andersen, Dannny Grunbaum and the entire crew of the *R/V Thompson*, whose hard work over many long nights made this study possible.

Abstract

Cross seamount, located off the coast of Hawaii in the Northern Pacific was the focus of an ADCP current survey over a period of 46 hours. CTD casts were also taken at various sites on and around the seamount. Relative vorticity was calculated for depths between 53.52m and 293.52m.

Whilst current plots seemed to indicate the presence of flow reversal at times, CTD data showed little evidence of any density structure anomalies associated with stable Taylor cap circulation. Relative vorticity values in the upper waters (above 150m) suggest anti-cyclonic vorticity (vorticity/f = -0.2172), whilst values below this depth suggest cyclonic vorticity (vorticity/f = 0.1667). Comparison of the Cross study site parameters to modelled values suggested the possible occurrence of temporarily trapped vortices.

Despite the suggestion of vorticity, little evidence was found to suggest the presence of a stable Taylor cap, with possible causes being the presence of a nearby cyclonic eddy, or the presence of orbiting satellite vortices.

Non-technical Summary

Seamounts are raised areas of seafloor in the ocean. When ocean currents and tides interact with seamounts, rotational flows often develop in the surface waters above the peak (known as Taylor caps or vortices). This study used a device called and ADCP to map currents at different depths above Cross seamount off the coast of Hawaii over the course of 46 hours. Profiles of water density were also taken on and off the seamount, looking for perturbations associated with the rotational flows above seamounts.

Parameters observed at Cross were compared to flow models with similar structures, to try and ascertain the likelihood of a Taylor cap existing. The results from this process suggest a regime where rotational motions may exist for periods of time above the seamount, but are ultimately unstable.

The current data collected were used to calculate the degree of rotation present in the waters above the seamount, ultimately finding little evidence of a Taylor cap. However, the presence of opposite rotation was also noted.

Introduction

Seamounts are areas of raised bathymetry, which occur throughout the world's oceans. They may be defined as tall (i.e. those which occupy a large portion of the total water depth), or they may occur as short seamounts, with a small vertical scale in comparison to water depth. Seamount shapes also vary dramatically, with flat-topped seamounts often being referred to as 'guyots'. Seamounts may occur in groups, sometimes in arc-like chains as a result of tectonic processes (Roden 1987).

Seamounts are significant areas in the world ocean in terms of biological (Brainard 1986; Dower et al. 1992; Noble and Mullineaux 1989), chemical (Wang and Dewar 2003) and geological processes (Keating 1987). Indeed, seamounts have been shown to have a significant effect upon ocean circulation patterns and thermohaline structure. Seamounts may also contribute to enhanced mixing (Eriksen 1995; Eriksen 1998), act to amplify tidal flows (Eriksen 1991), generate internal waves and eddies, and cause geopotential height perturbations [reported in (Roden 1987)].

Seamounts exist upon a rotating earth, within a stratified ocean. When an impinging current or other induced fluid motion interacts with a seamount, various flow features or phenomena may result.

These may include Taylor caps, sometimes referred to as Taylor columns. Here we use the former nomenclature, so as not to imply any particular shape or structure [following (Schär and Davies 1988) and (Chapman and Haidvogel 1992)], since these may vary due to local forcing conditions and bathymetry.

Taylor caps are anticyclonic vortices, which may form above a bathymetric feature, within which fluid can become entrapped (**Fig 1**). Taylor caps occur

where a steady current flows over a seamount or other topographic feature. The fluid column on the upstream side is compressed, whilst the column on the downstream side is stretched (Goldner and Chapman 1997). This leads to the formation of an anticyclonic and a cyclonic vortex, which then begin to co-rotate about the seamount (**Fig 2**). These vortices may persist for some time, and may be described as Taylor cap precursors.

Whether or not these precursor vortices develop into a Taylor cap is dependent on the incident current strength, and can be classified by means of the Rossby number (**Fig 3**), (Goldner and Chapman 1997). The Rossby number describes the ratio of inertial forcing to Coriolis forcing. When $R_0 << 1$, flow can be described as linear and geostrophic. At values around 0.3 and higher, flow can be described as turbulent and dominated by inertial forcing (Chapman and Haidvogel 1992; Pedlosky 1987).

In situations with strong incident flow [$R_0=O(1)$], the current may pass over the summit of the seamount, sweeping both vortices downstream. In situations where the incident flow is fairly weak, the cyclonic (downstream) vortex may be carried away, whilst the anticyclonic (upstream) vortex is pushed on top of the seamount, forming a Taylor cap.

Taylor caps and other rotational flow features may also form as a result of tidal forcing. Tidal currents can generate an oscillatory flow over the seamount, which when interacting with bathymetry may lead to the development of residual current structures about the seamount. Such features are often described as being a result of 'tidal rectification' (Codiga 1993; Kunze and Toole 1997). Features such as Taylor caps have been shown to have an effect upon biological processes (Boehlert and Genin 1987; Mullineaux and Mills 1997) as well as

physical processes (Lindsay et al. 2008) at seamount sites.

The chosen study site, Cross Seamount, is an ~85 Ma old Cretaceous guyot, located on the Hawaii-Emperor seamount trail at 18º 42.27' N 158º 15.97' W (**Fig 4**) (Wessel and Keating 1994). The summit of cross is located at a depth of 395m, with the local seafloor depth being around 4300m (Keating 1987; Noble and Mullineaux 1989).

Research into flow dynamics at other seamount sites (Eriksen 1991; Eriksen 1995; Mohn et al. 2009; Roden 1987), as well as work in modeling flow around topography (Chapman and Haidvogel 1992; Nycander and Lacase 2004), provide a basis for the study of flow at Cross.

I hypothesize that some rotational motion (seamount associated vorticity), probably anti-cyclonic, may exist around the summit of Cross. This may be a stable vortex, such as Taylor cap, which is permanently present above the seamount. Such a feature may be due to impinging flow, if it is stable in direction and magnitude over a timescale of several hours. Seamount associated vorticity may also be due to tidal rectification (Codiga 1993; Kunze and Toole 1997). However, the tall nature of Cross seamount may mean that such a stable vortex may not exist (Nycander and Lacase 2004). However, the presence of transient satellite vortices (resultant of vortex fission) and other flow features distinct from mean flow is quite probable.

Method

ADCP Data Collection

The ADCP unit of the *RV Thompson* is a hull-mounted Teledyne RD 75khz Ocean Surveyor. This instrument was used to collect continuous current velocity data at Cross seamount over a period of 46 hours. The range of this unit was from a depth of around 10m to a depth of 669m. However, it is important to note that the accuracy of ADCP readings close to bottom boundaries (within 6% of water depth) is very poor, due to the effect of side-lobe contamination (Muste et al. 2004). This effect is most evident above the summit at depths around 400m and close to the flanks of the seamount at depths below this.

A radial survey pattern was utilised, consisting of three major transect lines (of length 6 nautical miles) arranged so as to overlap at a point over the centre of the seamount (Point C). Each of these major spokes was connected to the next by lines between the endpoints (See **Fig 5**). This method was devised so as to provide continuous data collection over an entire survey, and to maximise spatial resolution at the study site. The location and designation of the end of each major spoke are given in **Table 1** (See **Figures and Results** section).

CTD Data Collection

CTD profiles were taken at 6 locations, on the seamount, upstream of the seamount and downstream of the seamount (see key in **Results** for positions, designations and relative locations). The data from these casts was used to generate density and buoyancy frequency, against depth plots (**CTD1-CTD5**).

Results

ADCP Data

Raw ADCP data files were processed using the MATLAB scripts 'load_getmat.m' and 'trackvec.m' (Eriksen, C., pers. comm.). The data were then divided into 6 surveys, with each survey constituting a full traverse of the pattern (from point 6 to point 1 in descending order). These profiles were then split into 3 depth bands, the upper depth band consisting of data between 29-109m, the mid-depth band comprised of data from 109-269m, and the deep band consisting of data from 269-669m. The data in the upper band were grouped into 40m depth bins, whilst data in the mid and deep layers were grouped into 80m depth bins.

It is important to note that at depths approaching the seamount summit (~400m), data becomes somewhat less reliable due to the proximity of measurements to the bottom boundary. Interference with bathymetry may also decrease the reliability of measurements taken in deeper water over the flanks of the seamount.

Current vector plots were produced for each survey (using trackvec.m), at all three band depths (upper, mid and deep). The plots generated are available in the attached **Figures and Results** section. Please refer to the key below for the name and description of each figure. Figures **Gif Up**, **Gif Mid** and **Gif Deep** refer to animated plots of all profiles at corresponding depth bands.

For an analysis and interpretation of these plots please refer to the Discussion section.

Survey Number	Start Time (D/M/Y)	End Time (D/M/Y)	Upper	Mid	Deep
Survey 1	2000GMT 31/12/2010	0015GMT 01/01/2011	**Plot 1.1**	**Plot 2.1**	**Plot 3.1**
Survey 2	0015GMT 01/01/2011	0645GMT 01/01/2011	**Plot 1.2**	**Plot 2.2**	**Plot 3.2**
Survey 3	0645GMT 01/01/2011	1245GMT 01/01/2011	**Plot 1.3**	**Plot 2.3**	**Plot 3.3**
Survey 4	1245GMT 01/01/2011	2000GMT 01/01/2011	**Plot 1.4**	**Plot 2.4**	**Plot 3.4**
Survey 5	2000GMT 01/01/2011	0925GMT 02/01/2011	**Plot 1.5**	**Plot 2.5**	**Plot 3.5**
Survey 6	0925GMT 02/01/2011	1812GMT 02/01/2011	**Plot 1.6**	**Plot 2.6**	**Plot 3.6**
All Surveys	2000GMT 31/12/2010	1812GMT 02/01/2011	**Plot 1**	**Plot 2**	**Plot 3**
All Surveys GIF	2000GMT 31/12/2010	1812GMT 02/01/2011	**Gif Up**	**Gif Mid**	**Gif Deep**

Relative Vorticity (ζ)

Relative vorticity is a measure of the rotation of a body of water, relative to the Earth. Relative vorticity can be used to assess the degree of rotation at a specific site, and its directionality. Positive values indicate anti-clockwise flow (cyclonic), whilst negative values denote clockwise flow (anticyclonic).

This approach has been utilised at other seamount study sites (Mohn et al. 2009).

Relative vorticity (ζ) is defined as;

$$\zeta = \frac{dv}{dx} - \frac{du}{dy} \qquad (1)$$

u and *v* at any location can be described using the following identities (C. Eriksen, pers. comm);

$$u = a + bx + cy + noise \qquad (2)$$
$$v = d + ex + fy + noise \qquad (3)$$

Where;

$$b = \frac{du}{dx} \qquad (4) \qquad c = \frac{du}{dy} \qquad (5)$$

$$e = \frac{dv}{dx} \qquad (6) \qquad f = \frac{dv}{dy} \qquad (7)$$

From these values, it is then evident that;

$$\zeta = e - c \qquad (8)$$

To find e and c , the following fits were calculated in MATLAB

$$\begin{bmatrix} u1 \\ u2 \\ u3 \\ u4 \\ u5 \\ u6 \\ u7 \end{bmatrix} = \begin{bmatrix} 1 & x1 & y1 \\ 1 & x2 & y2 \\ 1 & x3 & y3 \\ 1 & x4 & y4 \\ 1 & x5 & y5 \\ 1 & x6 & y6 \\ 1 & x7 & y7 \end{bmatrix} \begin{bmatrix} a \\ b \\ c \end{bmatrix} \qquad \begin{bmatrix} v1 \\ v2 \\ v3 \\ v4 \\ v5 \\ v6 \\ v7 \end{bmatrix} = \begin{bmatrix} 1 & x1 & y1 \\ 1 & x2 & y2 \\ 1 & x3 & y3 \\ 1 & x4 & y4 \\ 1 & x5 & y5 \\ 1 & x6 & y6 \\ 1 & x7 & y7 \end{bmatrix} \begin{bmatrix} d \\ e \\ f \end{bmatrix} \qquad (9)$$

Where x and y values are distances in metres from the origin (station 7), and numbered v and u values ($u1$, $u2$ …) are deviations from time averaged mean current at each station (1-7). Mean current at a given depth band was defined as being the average current in the u and v directions for all seven stations (**Table 3**).

MATLAB evaluation of these terms yielded values of c and e for each averaged depth layer. From these it was then possible to calculate relative vorticity at each averaged depth layer (**Table 3**). Relative vorticity was normalised to the localised Coriolis frequency (ζ/f), following the methods of a prior study at Sedlo seamount in the North Atlantic (Mohn et al. 2009). This data was then plotted against averaged depth (**Fig 6**). The data reveals strongest anticyclonic motion in the upper 150m of the water column (maximum value of -0.2172 at the shallowest bin), with cyclonic motion becoming the dominant mode at depths below 150m (maximum value of 0.1667)

The directionality and magnitude of deviations from mean current at each station are plotted as **Fig 7** (see **Figures and results**).

CTD Data

Six CTD casts were taken at sites upstream, downstream and on the summit of Cross seamount. Raw CTD data files were processed using SeaPlot (included in SeaBird Electronics' SeaSoft V2) to produce vertical profiles of density and buoyancy frequency against depth. Average buoyancy frequency and standard deviation were also calculated for each site using the MATLAB script 'ctd_rd.m' (Pawlowicz 1999). The plots generated are attached in the **Figures and Results** section. Please refer to the key below for station latitude, longitude, relative positions and designations, as well as calculated average buoyancy frequency (N) and standard deviation of the average N.

Name	Position	Latitude	Longitude	Average N	Std. Dev. N
CTD 1	Summit	18 42.86 N	158 15.98 W	5.3745	1.6832
CTD 2	Summit	18 42.77 N	158 15.91 W	5.1489	2.0312
CTD 3	NE Flank	18 43.73 N	158 14.49 W	3.9262	2.0368
CTD 4	SW Flank	18 41.33 N	158 18.48 W	4.0446	2.157
CTD 5	NE Flank	18 44.11 N	158 14.25 W	3.0495	2.0708

Discussion

CTD Data (see **Figures and results, CTD1- CTD5**)

Taylor caps may lead to enhanced vertical mixing, and the resultant genesis of a warm, light water mass above a cold, dense formation at the seamount summit (see **fig 8**) (Pitcher 2007) .

All CTD casts indicate the presence of greatest density stratification between 20-80m, both on and off-seamount. This would seem to indicate that any stratification present is resultant from a spatially uniform phenomena (such as insolation mediated heating) rather than any process occurring only at the seamount crest. Indeed, there is also very little difference in density structure

and stratification from sites upstream (**CTD4**) and those downstream (**CTD3** and **CTD5**).

Whilst the summit profiles (**CTD1** and **CTD 2**) show some small differences in density structure below this depth (80-200m), the variation is not significant enough to indicate a distinct temperature anomaly structure resultant from enhanced vertical transport due to the presence of a Taylor cap.

ADCP Data

Surface

The surface band of depths above Cross exhibit relatively steady uniform flows of around 0.4 m/s to the north-east (See **Plot 1- Plot 1.6**). These currents exhibit little change in directionality with time, and little variation in current speed. A decrease in average speed is noted for profile 4, and may be due to the effect of tidal forcing. The steady directional nature of surface currents is as expected, as vortices are often bottom-trapped and thus exhibit maximum effects at depth. Additionally, at shallower depths, the bathymetry of the seamount interferes less with impinging flow.

These northeasterly surface currents are mostly likely driven by the presence of a cyclonic eddy to the north.

Mid-depths

Currents observed in the mid-depth layer are far slower on average than those at the surface (0.1-0.2 m/s). The currents at these depths exhibit far less cohesion to an overall north-east flow. This cohesion decreases still further with depth (see **Plot 2.5**), with current directionality tending to the north with depth

(**Plot 2.1 -2.3**). This trend changes with time, as evidenced by **Plot 2.5,** where directionality with depth tends more to the east. This may again be due to the effect of the tide upon flow above the seamount. A significant decrease in current strength is noted for profile 6 (**Plot 2.6)** which may again coincide with a change in tidal state.

Profile 1, 2 and 6 show some evidence of flow convergence with depth in the northeast corner of the survey pattern (**Plot 2.1, 2.2 and 2.6**). This convergence occurs above a bathymetric feature at Cross, a depression in the northeast in the shape of a 'bite'. It is possible that this convergence may be driven by currents descending from the summit of the seamount and being channelled into this feature.

Whilst this layer exhibits more variance in terms of directionality and current than the surface, there is little sign of flow reversal at any point, one of the defining parameters for the presence of an anticyclonic Taylor cap.

Deep Layer

In the deeper band of depths, it is evident that flow is far less directional than at the surface (**Plot 3, 3.5 and 3.6)**. However, there is some indication that changes in directionality have a fairly uniform effect upon currents spatially (**Plot 3.3 and 3.4**).

Intensity of currents vary greatly with time between profiles (**plot 3.1 to plot 3.3**). Initially weak currents (~0.07 m/s) develop into stronger currents (0.35 m/s) with time. This may again be evidence of the effect of the tide upon flow above the seamount.

Plot 3.1, 3.5 and **3.6** show some sign of flow reversal, particularly in the west. This effect is greatest at depths between 269-350m, which may suggest the presence of some form of rotation. This would seem to agree with the theory that Taylor caps and other vortices above a seamount are bottom-trapped.

At depths greater than 350m, the current data becomes somewhat less reliable, as it approaches the bottom boundary, and side-lobe contamination becomes an issue. However, at the edges of the summit, especially to the East, an enhancement of flow and an abrupt change in directionality is seen (**Plot 3.5**). This may be due to the effect of bathymetry at the site interacting with impinging flow.

Comparison with theoretical model results

The effect of an impinging flow upon a tall seamount in a stratified ocean is a topic that has been given some considerable thought, especially in the realms of s-coordinate modelling (Chapman and Haidvogel 1992; Haidvogel et al. 1991). This work in modelling aimed to define the specific parameters at which a Taylor cap may form (**Fig 9**).

To define Rossby numbers (Ro) at Cross (**Fig 3)** we must first determine an average incident velocity (U) and a characteristic horizontal length scale (L). L for Cross is about 55km, whilst typical values of U in the surface waters at Cross range from around 0.1 m/s to 0.5 m/s. This in turn leads to calculated Rossby number values of 0.03 to 0.199 (see **Table 2**).

If we take the height of Cross to be 4050m, and the depth of the surrounding seafloor to be 4500m, it then becomes possible to calculate the

fractional height (δ) where $\delta = h_m/H$ (see **Fig 10**). A typical δ value for Cross is therefore in the region of 0.9.

If we consider these values and apply them to the model results in **Figure 9**, we can see that Cross occupies an interesting area in the graph. With a fractional height of 0.9, it is evident that Cross is a very tall seamount, approaching the limit of the theoretical model. Using the Rossby numbers derived in **Table 2**, we can see that Cross occupies positions below the line necessary for Taylor cap formation (Ro < 0.15) as well as those above which Taylor cap formation would be expected (Ro >0.15).

This result, would seem to support the theory that some degree of anticyclonic motion exists over Cross at times. Whilst the fractional height of Cross, and the effect of additional forcing factors (such as tidal oscillations and internal waves) precludes any assumption that temporary trapping (*TT*) is occurring as a regime, it is possible that variations in mean incident flow could be causing such an effect to manifest. However, it is important to note that the graph produced in **Figure 9** is based on models of Gaussian seamounts, and does not take into account the effect of the complex and unique variable bathymetry of a real-world seamount such as Cross. It is also important to recall that this study only examined steady incident flow upon a seamount, and not the oscillatory flows associated with tidal rectification.

Relative Vorticity

Relative vorticity data from Cross suggest a shift from anticyclonic surface currents to cyclonic deep currents at ~150m (See **fig 6**). This is contrary to the expected existence of anticyclonic flow at depth, as would be anticipated for a

Taylor cap. Indeed, by looking at the deviation from mean current (**Fig 7),** this shift to a more cyclonic flow with depth is visible.

It is clear from **Fig 6** and **Fig 7** that the largest magnitude deviations from mean flow are in the surface and bottom layers. Surface deviations however, are somewhat greater in magnitude than those at depth (-0.2172 vs +0.1667). This suggests that they may be driven by the strong surface currents observed in the upper waters (**see plot 1**).

The values of relative vorticity/f are similar to those in literature (~±0.05) (Mohn et al. 2009), but at times are somewhat greater. This may be due to the amplifying effect of the very tall height of Cross upon forcing factors, such as the tidal component (Eriksen 1991) and impinging flows.

Conclusion

The ADCP vector plot data seem to suggest the presence of flow reversal at times above Cross, especially at depth (see **Plot 3.1, 3.5 and 3.6**) This is one of the defining characteristics of the presence of a vortex, such as a Taylor cap. However, the direction of vorticity is contrary to that which would be expected for a Taylor cap (anti-cyclonic flow). Taylor caps are often bottom trapped, displaying strongest circulations at depths near the bottom boundary feature (Codiga 1993; Nycander and Lacase 2004). However, at Cross, circulations at depths near the seamount summit (~350m) displayed positive relative vorticity (**fig 6**), which would seem to suggest a cyclonic motion. However, it must be noted that data near the bottom boundary interface are more susceptible to side-lobe contamination and the effects of interference with bathymetry, though it is unlikely that such an effect would yield such a coherent shift in vorticity.

I conclude that there is little evidence to support the theory that a Taylor cap exists above Cross, at least as a stable feature. It is probable that the contrary relative vorticity values calculated were a result to the limited temporal nature of the dataset, especially when compared to the timescales of months employed by other studies (Mohn et al. 2009). Indeed, the occurrence of temporary positive vorticity anomalies above a seamount in place of the negative mode have been noted for periods of up to 30 days (Mohn et al. 2009). It may be during the sampling timeframe employed by this study, a similar cyclonic mode was dominant. One suggested reason for this change of mode was the occurrence of a change in background flow, evidenced by satellite altimetry data (Mohn et al. 2009). It may be possible that the motion of the nearby eddy to the north was responsible for such a shift at Cross.

Nycander et. al. noted the presence of stable and unstable vortices about especially tall seamounts. Model-based research shows fission of vortices above tall seamounts as contributing to the genesis of satellite and ancillary vortices, which often rotate clockwise about the summit (Nycander and Lacase 2004). It may be possible that similar processes may be occurring at Cross, leading to the genesis of unexpected flow features, such as the cyclonic bottom vorticity observed. If satellite vortices were present, their motions about the seamount may have caused them, at times, to impinge upon the area of our survey, potentially leading to the variability in current directionality seen at depth. This may also go some way towards explaining the curious nature of the mean cyclonic deviation from mean current at depth (**Plot 3.1, 3.5 3.6**).

Also, the tall nature of Cross (δ=0.9), means that it approaches the limit of s-coordinate modelling (Chapman and Haidvogel 1992; Haidvogel et al. 1991). This suggests that flow regimes above such a seamount are somewhat less predictable than at shorter seamounts. The large relative height of Cross, when coupled with unusual current regimes may act to destabilise any stable features, leading to a succession of temporary vortices induced by non-linear interactions with the seamount (Nycander and Lacase 2004; Pitcher 2007). CTD plots show little evidence of a dense cold water dome above the seamount summit, which has often been associated with stable vortices (Pitcher 2007).

In future, to achieve a more conclusive dataset, it would be extremely desirable to utilise an array of fixed-point current monitoring devices (such as hydrographic moorings and bottom-mounted ADCPs) over a timescale of several months. This would allow for a more accurate temporal and spatial representation of the processes occurring at Cross.

References

Boehlert, G., and A. Genin. 1987. A review of the effects of seamounts on biological processes. Seamounts, islands and atolls**:** 319-334.

Brainard, R. E. 1986. Fisheries aspects of seamounts and Taylor columns. NAVAL POSTGRADUATE SCHOOL.

Chapman, D. C., and D. B. Haidvogel. 1992. Formation of Taylor caps over a tall isolated seamount in a stratified ocean. Geophysical & Astrophysical Fluid Dynamics **64:** 31 - 65.

Codiga, D. L. 1993. Laboratory Realizations of Stratified Seamount-trapped Waves. Journal of Physical Oceanography **23:** 2053-2071.

Dower, J., H. Freeland, and K. Juniper. 1992. A strong biological response to oceanic flow past Cobb Seamount. Deep Sea Research Part A. Oceanographic Research Papers **39:** 1139-1145.

Eriksen, C. 1991. Observations of Amplified Flows Atop a Large Seamount. J. Geophys. Res. **96:** 15227-15236.

Eriksen, C. 1995. Waves, Mean Flows, and Mixing at a Seamount, p. 1. School of Ocean and Earth Science and Technology.

Eriksen, C. 1998. Internal wave reflection and mixing at Fieberling Guyot. J. Geophys. Res. **103:** 2977-2994.

Goldner, D. R., and D. C. Chapman. 1997. Flow and particle motion induced above a tall seamount by steady and tidal background currents. Deep Sea Research Part I: Oceanographic Research Papers **44:** 719-744.

Haidvogel, D. B., J. L. Wilkin, and R. Young. 1991. A semi-spectral primitive equation ocean circulation model using vertical sigma and orthogonal curvilinear horizontal coordinates. Journal of Computational Physics **94:** 151-185.

Keating, B. 1987. Seamounts, islands, and atolls. Amer Geophysical Union.

Kunze, E., and J. M. Toole. 1997. Tidally Driven Vorticity, Diurnal Shear, and Turbulence atop Fieberling Seamount. Journal of Physical Oceanography **27:** 2663-2693.

Lindsay, R. W., R. Kwok, L. De Steur, and W. Meier. 2008. Halo of ice deformation observed over the Maud Rise seamount. Geophys. Res. Lett. **35:** L15501.

Mohn and others 2009. Dynamics at an elongated, intermediate depth seamount in the North Atlantic (Sedlo Seamount, 40° 20'N, 26° 40'W). Elsevier.

Mullineaux, L. S., and S. W. Mills. 1997. A test of the larval retention hypothesis in seamount-generated flows. Deep Sea Research Part I: Oceanographic Research Papers **44:** 745-770.

Muste, M., K. Yu, T. Pratt, and D. Abraham. 2004. Practical aspects of ADCP data use for quantification of mean river flow characteristics; Part II: fixed-vessel measurements. Flow Measurement and Instrumentation **15:** 17-28.

Noble, M., and L. S. Mullineaux. 1989. Internal tidal currents over the summit of cross seamount. Deep Sea Research Part A. Oceanographic Research Papers **36:** 1791-1802.

Nycander, J., and J. H. Lacase. 2004. Stable and unstable vortices attached to seamounts. Journal of Fluid Mechanics **507:** 71-94.

Pawlowicz, R. 1999. CTD_RD. *In* ctd_rd.m [ed.].

Pedlosky, J. 1987. Geophysical fluid dynamics. Springer.

Pitcher, T. J. 2007. Seamounts: ecology, fisheries & conservation. Blackwell Pub.

Roden, G. I. 1987. Effect of seamounts and seamount chains on ocean circulation and thermohaline structure. Seamounts, islands and atolls**:** 335-354.

Schär, C., and H. C. Davies. 1988. Quasi-geostrophic stratified flow over isolated finite amplitude topography. Dynamics of Atmospheres and Oceans **11:** 287-306.

Wang, G., and W. K. Dewar. 2003. Meddy-Seamount Interactions: Implications for the Mediterranean Salt Tongue. Journal of Physical Oceanography **33:** 2446-2461.

Wessel, P., and B. H. Keating. 1994. Temporal variations of flexural deformation in Hawaii. J. Geophys. Res. **99:** 2747-2756.

Figure 1 – Visual representation of flow about a seamount (Mullineaux and Mills, 1997)

Fig. 3. Three-dimensional diagram of mean flows in the tidally rectified circulation cell, showing the character of azimuthal (clockwise, decreasing in strength with height above bottom), radial (strongly outward at the seamount summit, weaker and inward above), and vertical (strongly downward at the center, weaker and upward at periphery) flows. Diagram is not to scale; e.g. horizontal flows are much stronger than vertical ones.

Figure 2 – Precursor eddies and Taylor cap dynamics

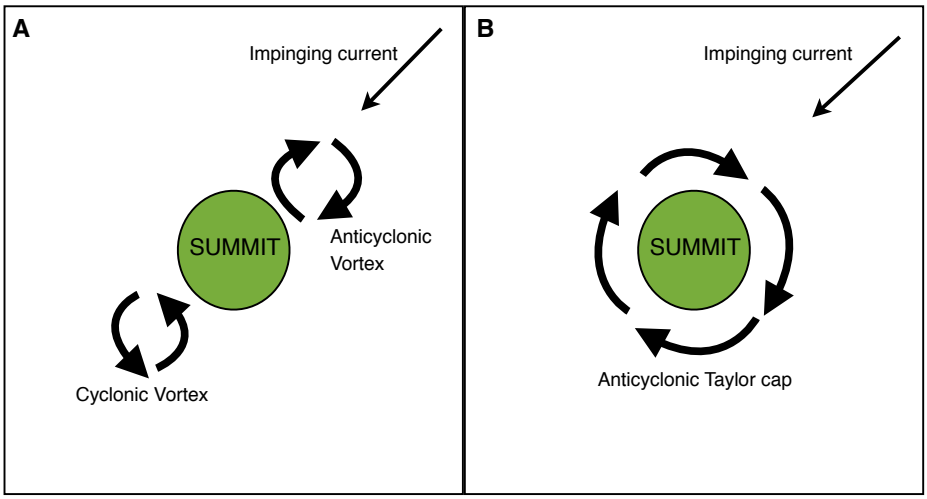

Panel A shows the development of two vortices, one cyclonic (downstream) and anticyclonic (upstream) as a result of a steady impinging current from the NE. These vortices may then begin to co-rotate about the seamount summit, and may be described as precursors to the formation of a Taylor cap. If the incident current strength is great enough, where [$\mathbf{R_0 = O(1)}$], the flow will move over the summit of the seamount, sweeping both vortices downstream. If the flow is relatively weak, only the downstream (cyclonic) vortex will be carried away, whilst the upstream (anticyclonic) vortex will move to occupy a position above the summit, forming a Taylor cap (**Panel B**).

Figure 3 - The Rossby equation, with Coriolis parameter localised for Cross seamount.

$\mathbf{R_0 = U/fL}$	U= Incident velocity f= Coriolis parameter (0.465×10^{-4} S^{-1}) L= Horizontal length parameter

Figure 4 - Location of Cross Seamount (Image from EarthRef Seamount Database - http://earthref.org)

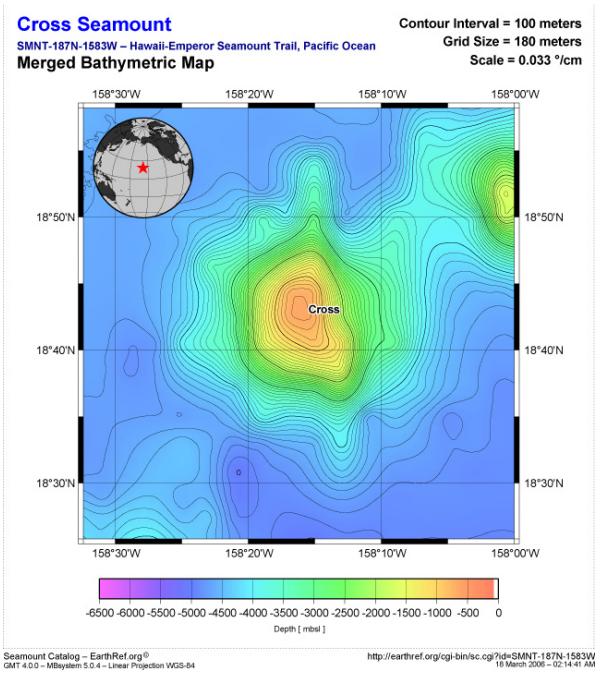

Figure 5 - Bathymetric chart of Cross seamount study site. The survey pattern is indicted in black. End of line points are numbered 1-6, with the centre point as C.

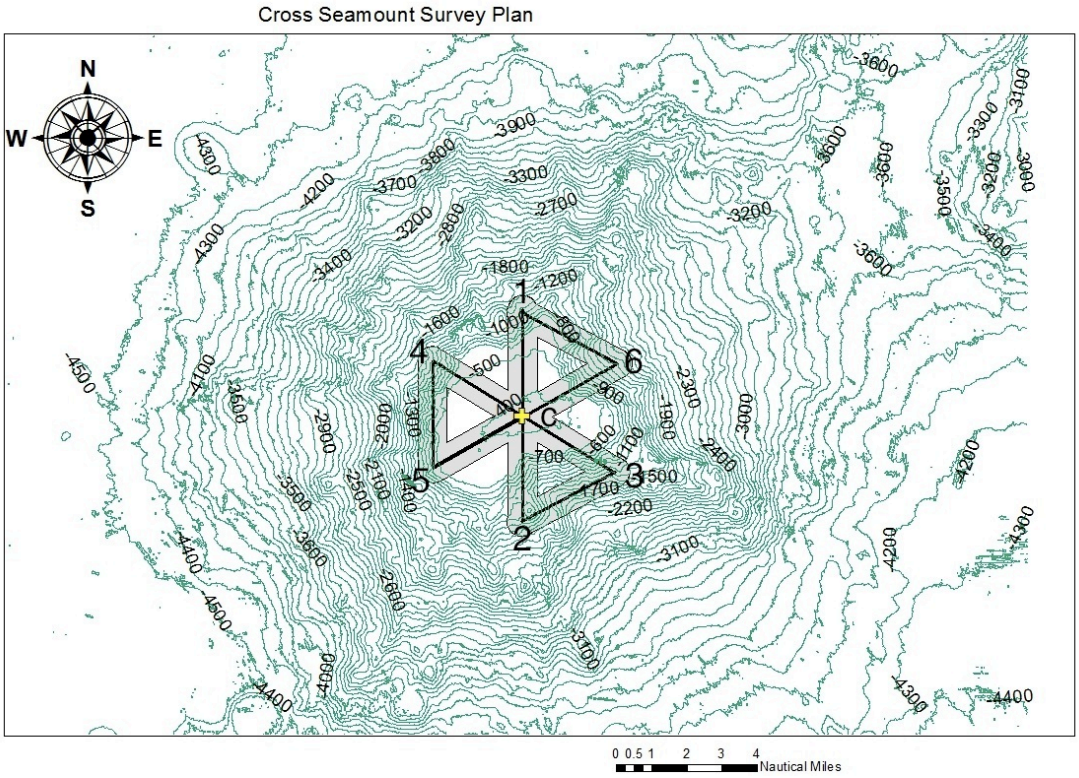

Figure 6 - Relative vorticity (normalised to local Coriolis frequency) against depth over theduration of the study.

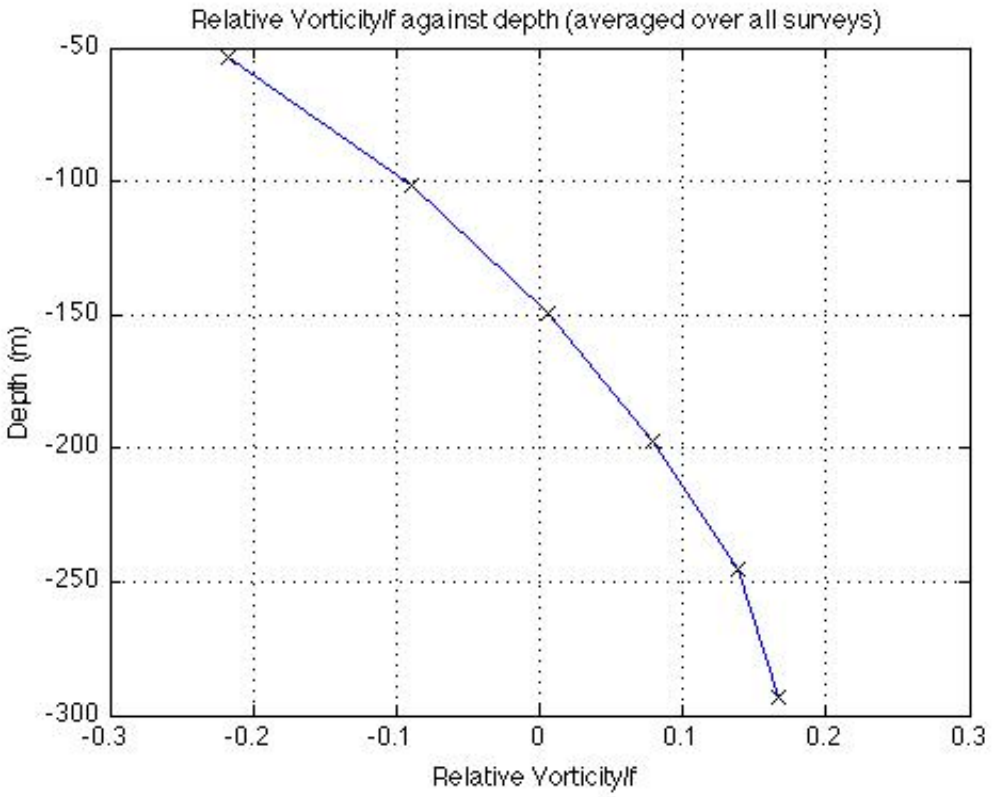

Figure 7 Deviations from mean current at stations 1-7

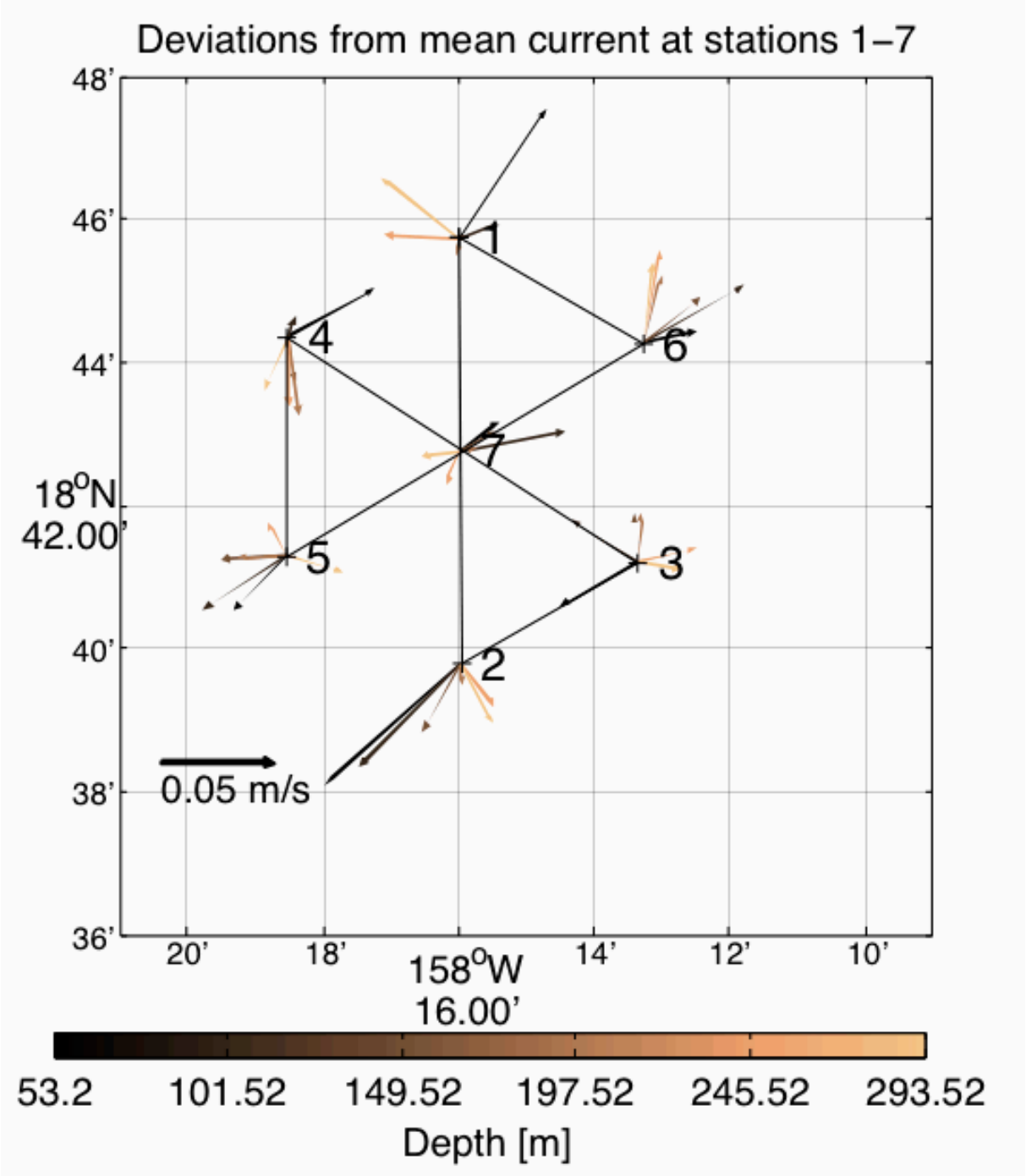

Figure 8 - A diagram showing enhanced vertical mixing and circulation due to upwelling at the edge of the seamount summit. Cross and dot show opposite flow directions. Ekman transport off the summit is evidenced by dashed lines. (Taken from Pitcher, 2007.)

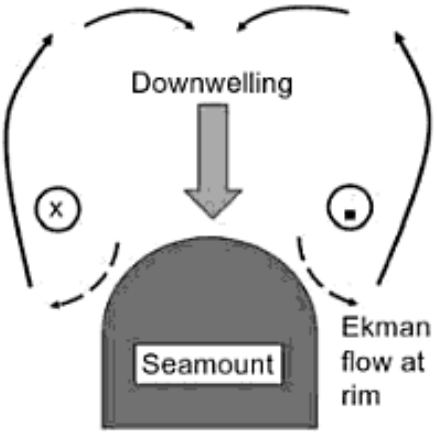

Figure 9 – Results of modelling steady stratified flow over a tall Gaussian seamount defined by fractional height and Rossby number. Flows above the heavy line move directly over the seamount, leaving no Taylor cap. The region marked *TT* indicates range of parameters in which 'temporary trapping' of flow may occur (Taken from Chapman and Haidvogel, 1992).

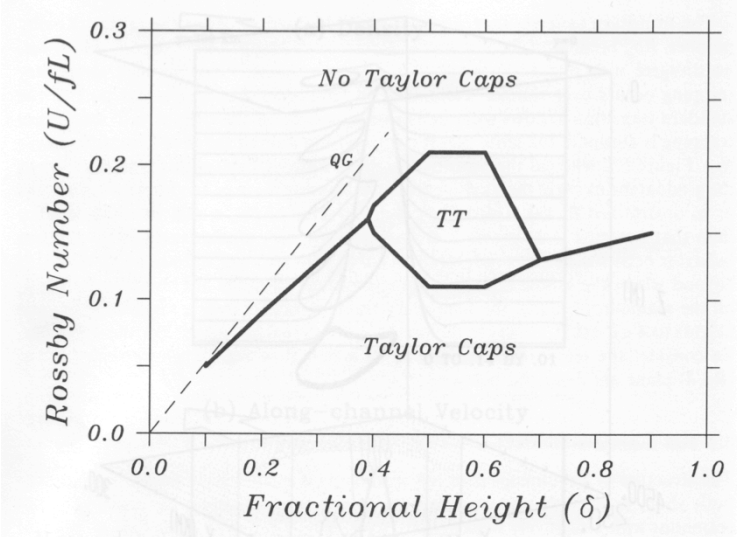

Figure 10 - Figure showing seamount height (h_m) and depth (H) (Chapman and Haidvogel, 1992).

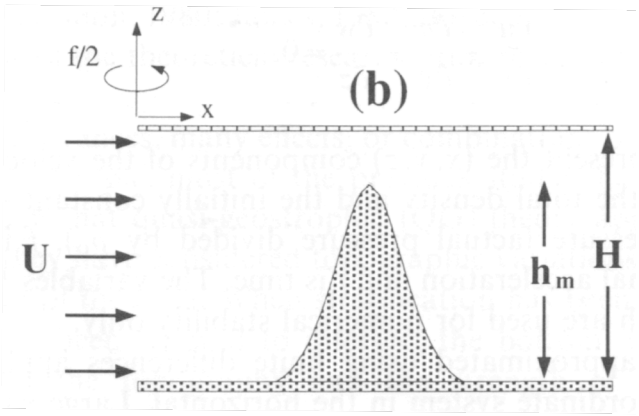

$\delta = h_m/H$

δ at Cross is around **0.9**

Table 1 – Location and designation of radial end-points (1-6) and the centre point (C)

Point	Latitude	Longitude
C	18 42.749 N	158 15.989 W
1	18 45.726 N	158 15.989 W
2	18 39.794 N	158 15.989 W
3	18 41.207 N	158 13.354 W
4	18 44.355 N	158 18.515 W
5	18 41.293 N	158 18.515 W
6	18 44.269 N	158 13.354 W

Table 2 – Calculated Rossby numbers for Cross seamount

Rossby Number	U (m/s)	F (Coriolis parameter)	L (metres)
0.039872408	0.1	0.0000456	55000
0.079744817	0.2	0.0000456	55000
0.119617225	0.3	0.0000456	55000
0.159489633	0.4	0.0000456	55000
0.199362041	0.5	0.0000456	55000

Table 3 - Relative vorticity and mean U and V values (from data binned at each station point) at Cross. Depths are averaged for the stated bin ranges.

Depth Bins Averaged	Depth (metres)	Mean U (total)	Mean V (total)	Vorticity	Vorticity/f
1 - 6	-53.2	0.121172936	0.146379425	-1.01E-05	-0.2172
7 - 12	-101.52	0.148248099	0.16806032	-4.13E-06	-0.0887
13 - 18	-149.52	0.093543803	0.111358976	2.89E-07	0.0062
19 - 24	-197.52	0.05909088	0.079960884	3.67E-06	0.0787
25 - 30	-245.52	0.051557608	0.058967333	6.46E-06	0.1387
31 -36	-293.52	0.032973525	0.051268881	7.77E-06	0.1667

CTD Plots

CTD 1-Summit

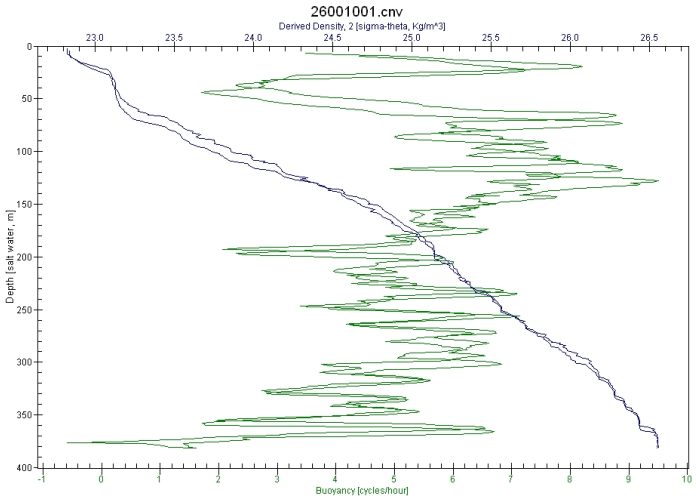

CTD 2 - Summit

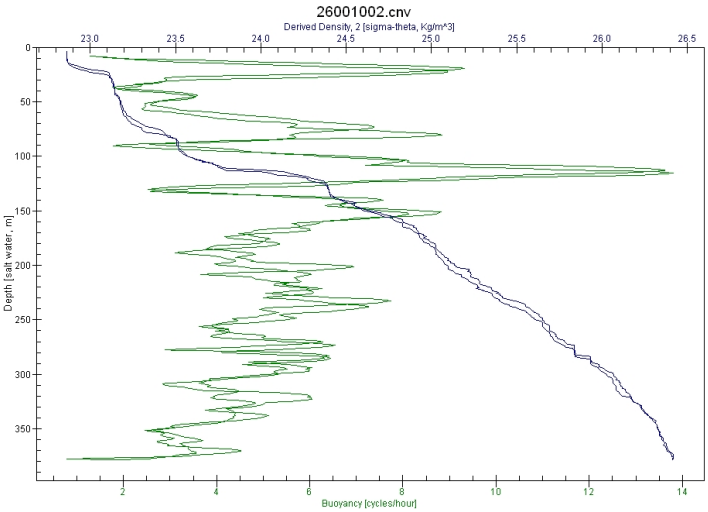

CTD 3 – NE Flank

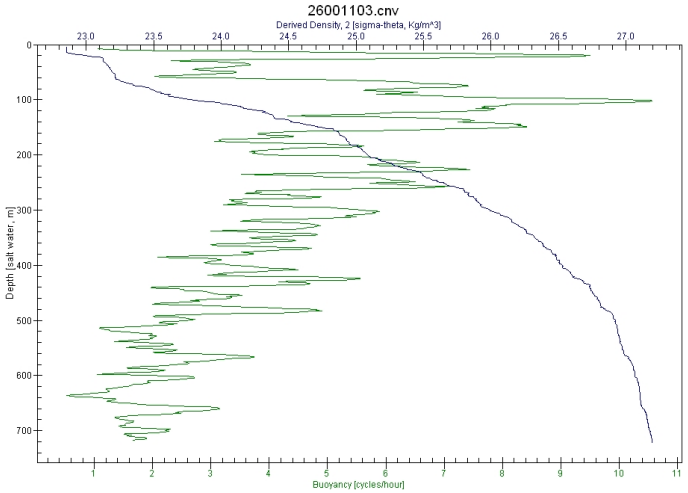

CTD 4 – SW Flank

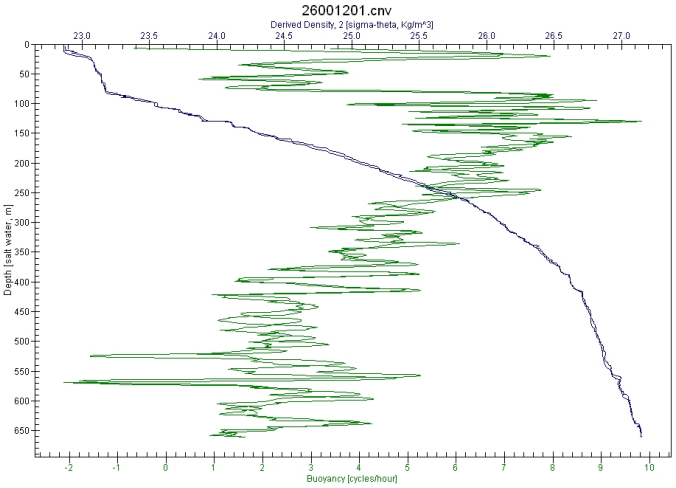

CTD 5 – NE Flank

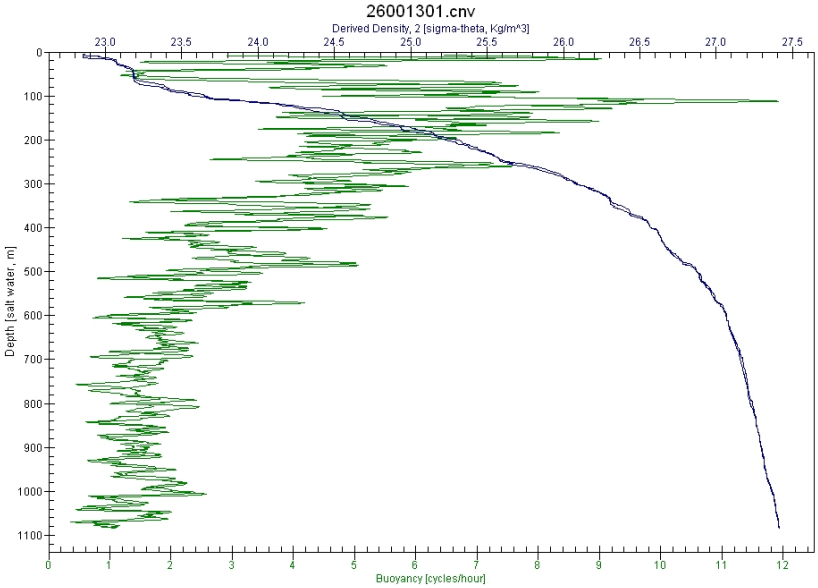

ADCP PLOTS

Plot 1.1

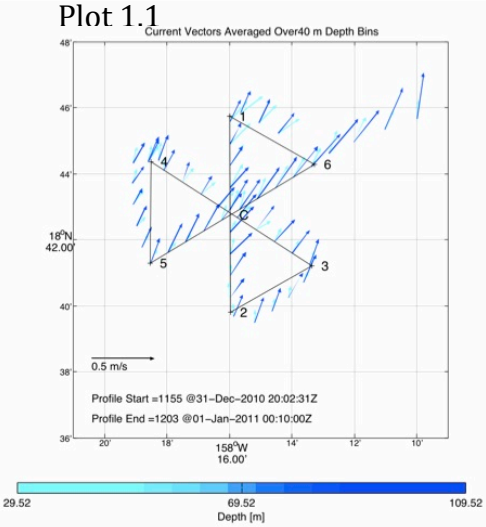

Plot 1.2

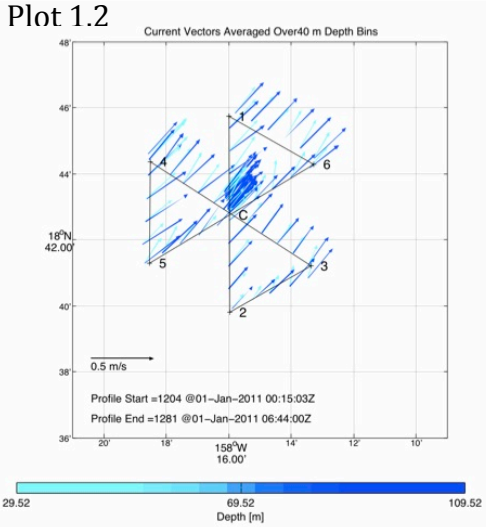

Plot 1.3

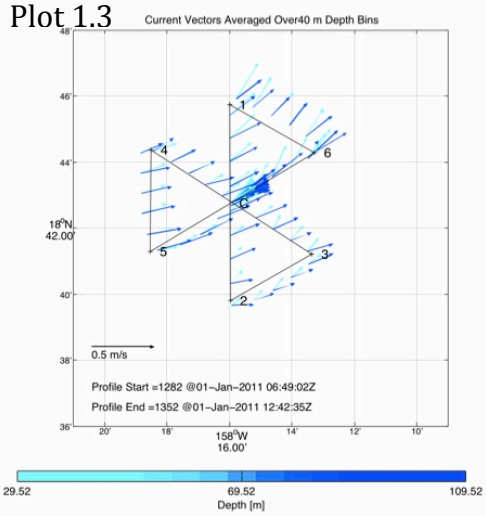

Plot 1.4

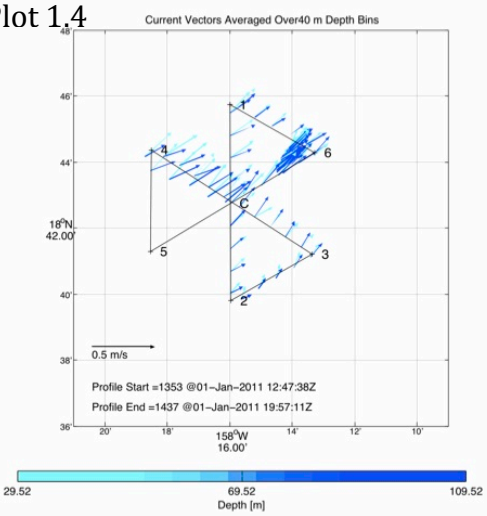

Plot 1.5

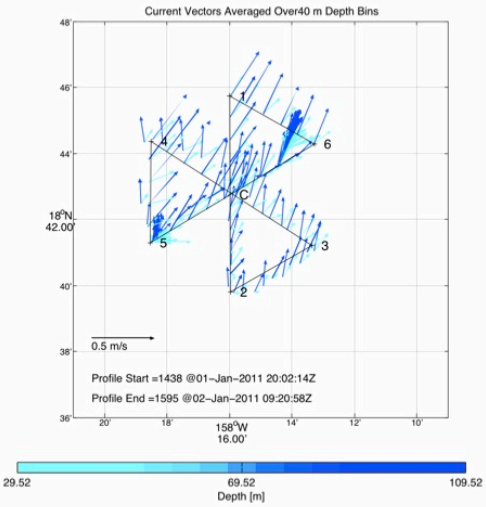

Plot 1.6

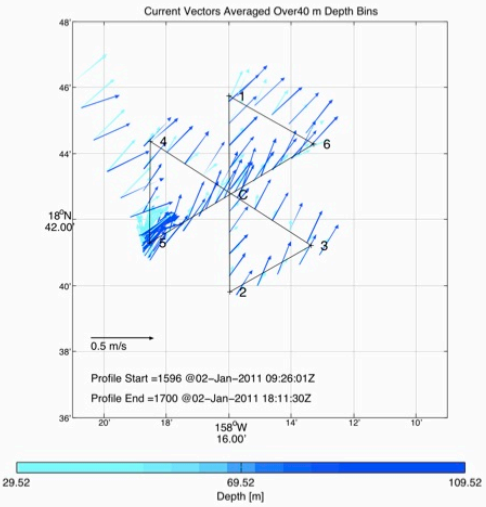

Plot 1

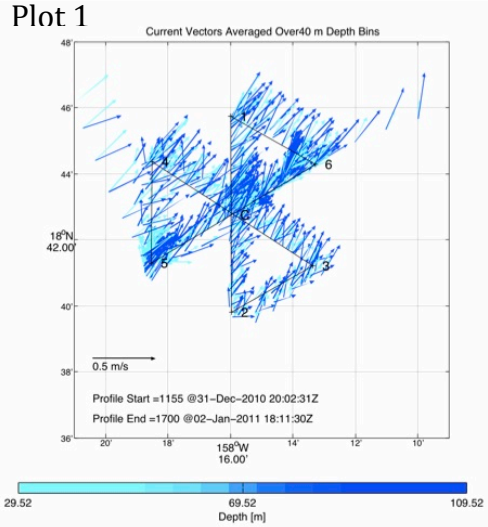

Plot 2.1

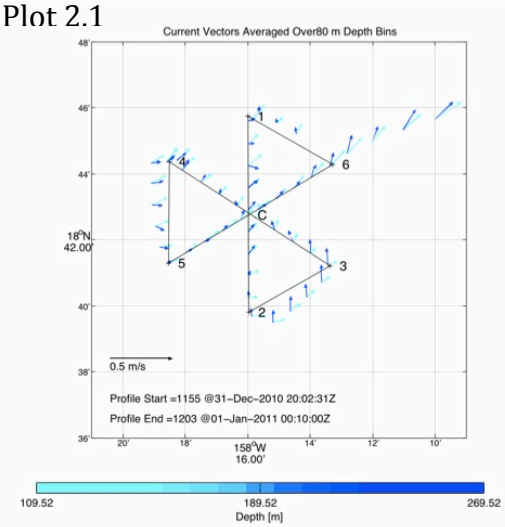

Plot 2.2

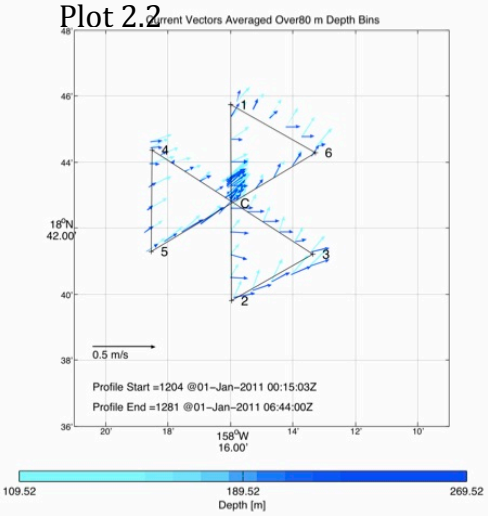

Plot 2.3

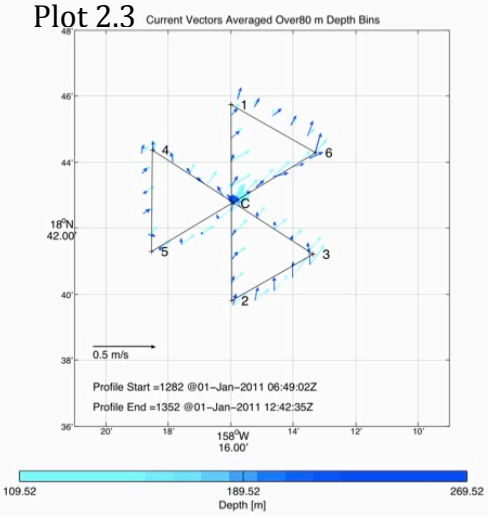

Plot 2.4

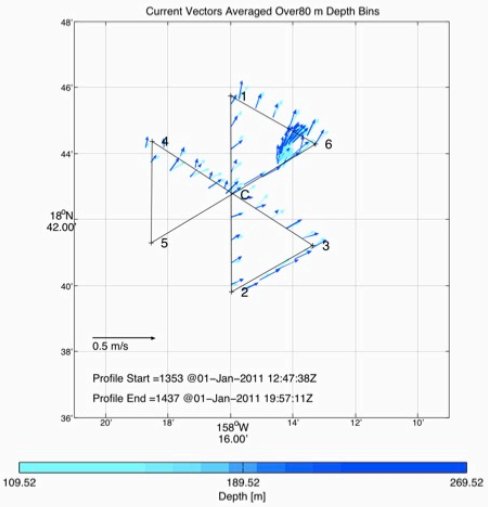

Plot 2.5

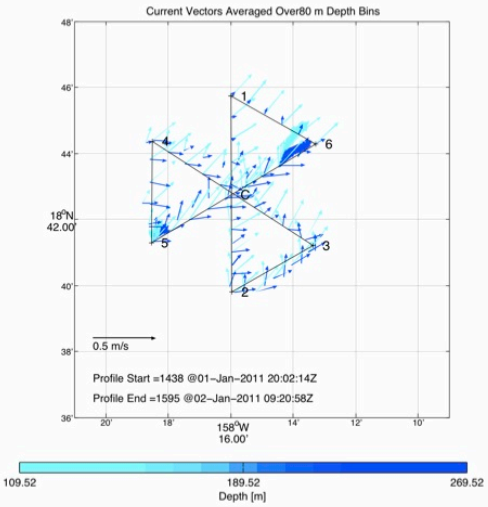

Plot 2.6

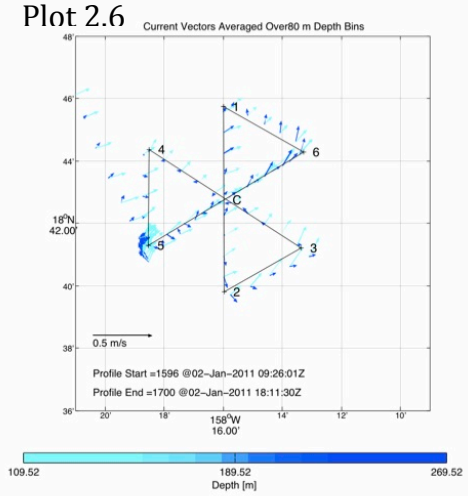

Plot 2

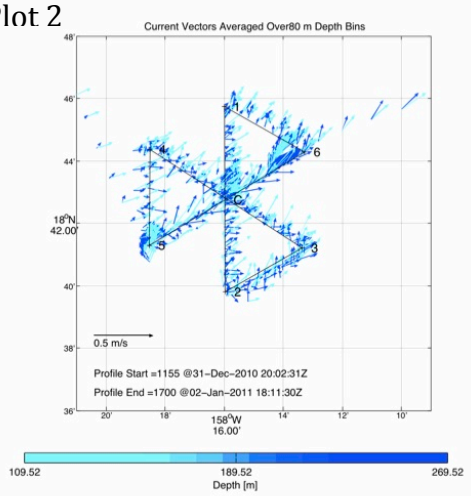

Plot 3.1

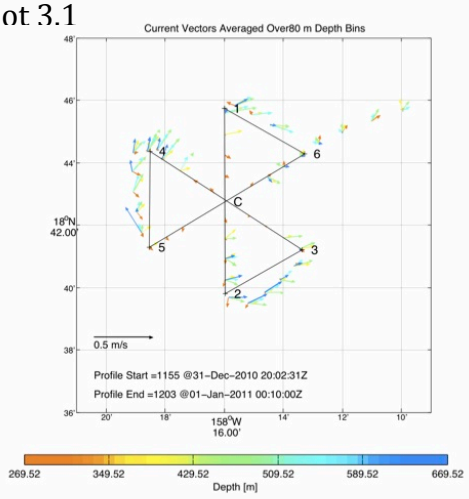

Plot 3.2

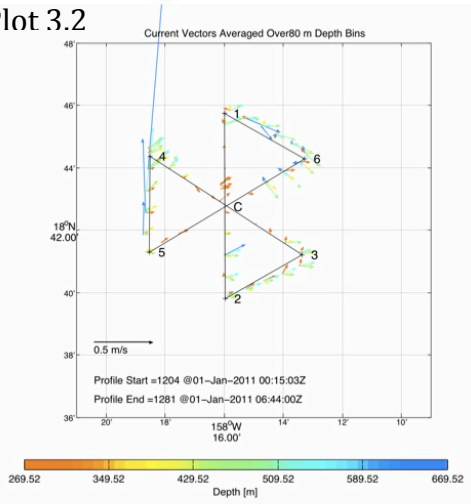

Plot 3.3

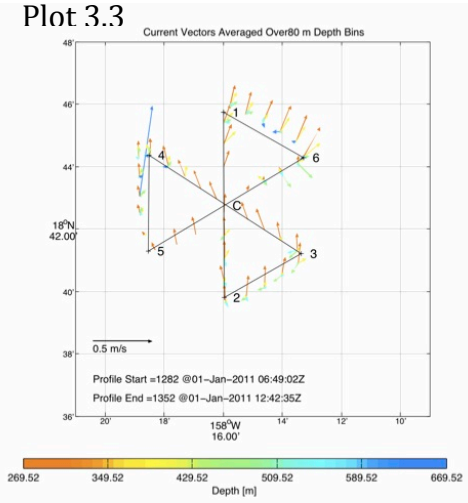

Plot 3.4

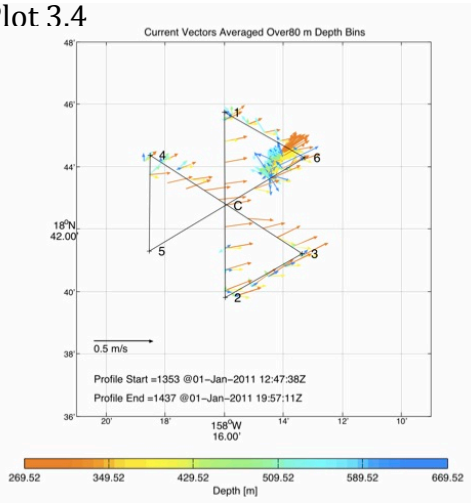

Plot 3.5

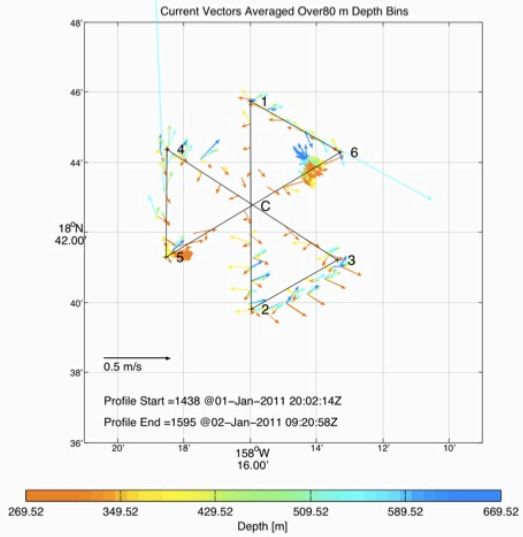

Plot 3.6

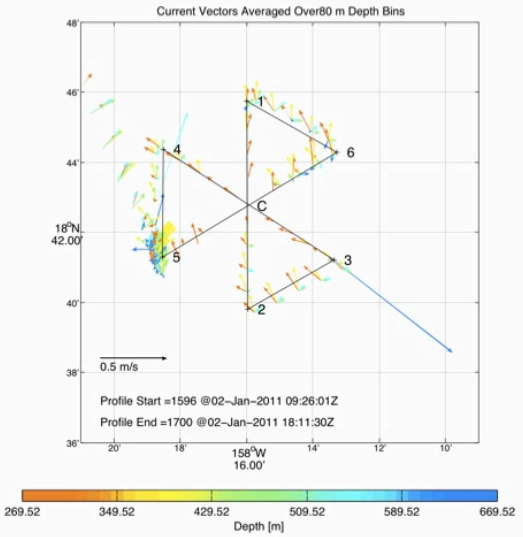

Plot 3